

# Quasiperiodic gallium adlayer on *i*-Al-Pd-Mn

Pramod Bhakuni<sup>1</sup>, Marian Krajčí<sup>2,\*</sup>, Sudipta Roy Barman<sup>1,†</sup>

<sup>1</sup>*UGC-DAE Consortium for Scientific Research, Khandwa Road, Indore - 452001, Madhya Pradesh, India and*

<sup>2</sup>*Institute of Physics, Slovak Academy of Sciences,  
Dúbravská cesta 9, SK-84511 Bratislava, Slovak Republic*

Using scanning tunneling microscopy (STM), low energy electron diffraction (LEED), and density functional theory (DFT), we demonstrate the formation of quasicrystalline gallium adlayer on icosahedral (*i*-Al-Pd-Mn). Quasiperiodic motifs are evident in the STM topography images, including the Ga white flower (GaWF) and  $\tau$  inflated GaWF ( $\tau$ -GaWF), where  $\tau$  is the golden mean. A larger and more complicated ring motif is also identified, comprised of a bright center and an outer ring of pentagons. The fast Fourier transform of the STM images exhibits distinct quasiperiodic spots, thereby establishing quasiperiodicity on a length scale of  $\sim 350$  nm. Based on our DFT calculations, the preferred adsorption sites of Ga on *i*-Al-Pd-Mn are determined to be either the Mn atoms at the center of the Penrose P1 tile or the vertices of the P1 tile containing Pd atoms at the center of a cluster of 5 Al atoms (5-Al). The GaWF motif is modeled by an inner 6 atom Ga cluster (6-Ga) around the central Mn atom and an outer ring of 5 Ga atoms adsorbed at the centers of the 5-Al clusters, both having pentagonal symmetry. The  $\tau$ -GaWF motif is modeled by the 6-Ga arranged on the  $\tau$ -P1 tiling, while the ring motif is modeled by Ga atoms adsorbed at the center of 5-Al clusters above a Pd atom. The side lengths and diameters of the GaWF,  $\tau$ -GaWF, and the ring motifs are  $\tau$  scaled and show excellent agreement with the DFT-based models. An additional indication of the quasiperiodic characteristics of the Ga monolayer is the 5-fold LEED patterns that were detected throughout the entire range of beam energy that was measured.

## I. INTRODUCTION

Quasicrystals are a distinct type of material that display aperiodic order with rotational symmetries, including 5-fold, 8-fold, 10-fold, and 12-fold, which are forbidden in crystals with translational order [1, 2]. The quasicrystalline phase was first identified in a binary alloy of Al<sub>6</sub>Mn with icosahedral symmetry [3], and since then it has been observed in a variety of systems, which include ternary and binary intermetallic compounds [4], nanoparticle superlattices [5], colloidal systems [6], perovskite barium titanate on Pt(111) [7], molecular assemblies [8, 9], twisted bilayer graphene [10–12], chalcogenides [13], elemental films [14–17], and even in naturally occurring minerals [18, 19]. Inorganic quasicrystals exhibit unusual properties such as low thermal and electrical conductivity, low specific heat, low frictional coefficient, and large hardness [20–24]. Their stability has been related to the pseudogap i.e., a reduced density of states (DOS) around the Fermi level [25–28]. The possibility of higher order topological states occurring in quasiperiodic systems has been predicted by theory [29–31]. Our recent research utilizing hard x-ray photoemission spectroscopy and density functional theory (DFT) has established the occurrence of Anderson localization in icosahedral (*i*-Al-Pd-Re [32]).

Since more than two decades, researchers have studied elemental quasicrystalline films to investigate the impact of aperiodic order on the physical and electronic properties that are independent of the chemical complexity of the ternary quasicrystals. But to date, only a few elements have demonstrated quasiperiodicity [14–17, 33–40]. Franke *et al.* discovered that Bi and Sb are quasiperiodic on *i*-Al-Pd-Mn and decagonal Al-Ni-

Co quasicrystalline substrates up to 1 monolayer (ML) coverage using low energy electron diffraction (LEED) and He atom scattering [14]. Shukla *et al.* [39] showed that Na forms a regular 5-fold quasiperiodic bilayer on *i*-Al-Pd-Mn. Pb/*i*-Ag-In-Yb was reported to exhibit 5-fold growth isostructural with the *i*-Ag-In-Yb substrate to a maximum height of 0.7 nm [15]. Recent research utilizing scanning tunneling microscopy (STM), LEED, and DFT has demonstrated that a 4 nm thick Sn adlayer deposited on the fivefold surface of an *i*-Al-Pd-Mn substrate exhibits long range quasiperiodic order as a metastable realization of an elemental, clathrate family quasicrystal [16]. Long range decagonal clathrate quasiperiodic ordering of Sn thin films on *d*-Al-Ni-Co has also been observed up to 0.9 nm, with partial retention of decagonal structural correlations up to 10 nm film thickness [17].

Gallium is an interesting element due to its relatively low melting point (303 K) and its complex solid-state structure. The latter produces a notable dip at the Fermi level ( $E_F$ ), which is believed to be the consequence of partial covalent bonding [41, 42]. Recently, gallanene i.e., a honeycomb monolayer of Ga that is analogous to graphene, has been reported [43–47]. However, Ga deposition on single crystalline metal surfaces has been scarcely studied [48], and there has been no study on any quasicrystalline substrates to date. Ga could be a possible candidate since its surface energy (0.55 J/m<sup>2</sup>) [49] is less than that reported for the *i*-Al-Pd-Mn surface (0.82 J/m<sup>2</sup>) [50], indicating the possibility of layered growth. In this work, we use STM, LEED, and density functional theory (DFT) to reveal the occurrence of long range quasiperiodicity in a gallium monolayer deposited at room temperature (RT) on *i*-Al-Pd-Mn. The quasiperiodic motifs such as Ga white flower (GaWF),

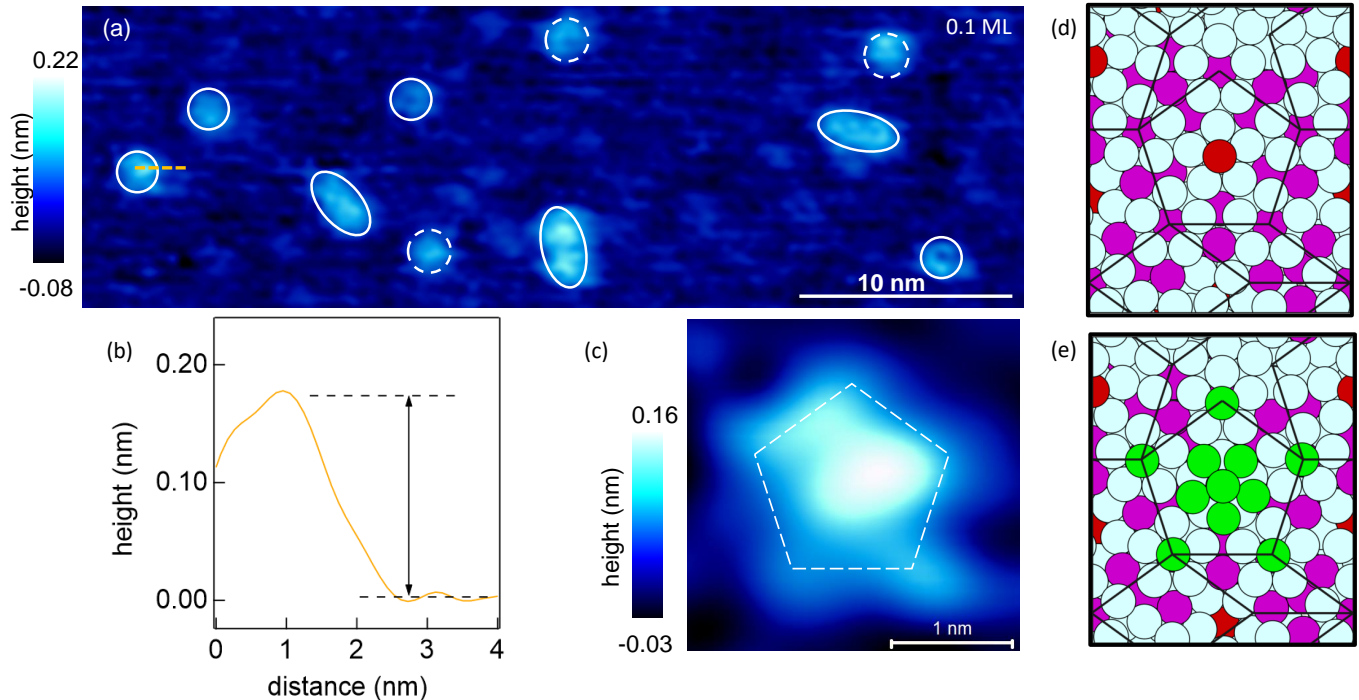


FIG. 1. (a) STM topography image of 0.1 ML Ga/*i*-Al-Pd-Mn ( $I_T = 0.9$  nA ,  $U_T = -0.7$  V) showing the Ga white flower (GaWF) motifs encircled by white circles and ovals, dashed circles show the incomplete motifs. The color scale representing the height is shown on the left, zero corresponds to the bearing height. (b) A height profile across the GaWF along the orange dashed line in panel a. (c) Zoomed view of a GaWF motif with a white dashed pentagon overlaid on it. (d) The atomic structure of the surface plane (2.3 nm $\times$ 2.4 nm) of the 5-fold *i*-Al-Pd-Mn derived from the 2/1 approximant to the bulk. The white, magenta, and red colored circles represent the Al, Pd, and Mn atoms, respectively. The Penrose P1 tiling is shown by black lines. (e) An 11 Ga atom DFT based model of the GaWF centered on the Mn site of the 5-fold *i*-Al-Pd-Mn. The green colored circles represent the Ga atoms.

$\tau$  scaled GaWF ( $\tau$ -GaWF), and the ring observed from STM have been modeled by our DFT calculations. The fast Fourier transform of the large area STM images exhibits distinct quasiperiodic spots.

## II. METHODS

The STM measurements were carried out using a variable temperature STM from Scientaomicron GmbH at a base pressure of  $5 \times 10^{-11}$  mbar. All the STM measurements were performed at RT in the constant current mode using a tungsten tip that was prepared by sputtering and the voltage pulse method. The tip was biased, and the sample was kept at the ground potential. STM images were recorded for varying bias voltages. The Fast Fourier transform (FFT) was averaged for 2-4 STM images, as in our previous work [17]. The STM images are shown after low-pass Fourier transform filtering (Fig. S1 of the Supplementary material (SM) [51]). The zero in the z-scale of the STM image corresponds to the most frequently occurring height (bearing height) based on the height histogram. In a height profile, the difference of the average  $z$

corrugation on the Ga adlayer and the substrate provides the height of the former [52]. The average height for a particular deposition is determined by fitting a Gaussian curve to the height distribution obtained from more than 50 height profiles derived from various parts of the STM images. LEED and AES were performed using a four-grid rear view optics and a hemispherical retarding field analyzer, respectively. The  $I$ - $V$  curves were extracted using the EasyLeed software [53].

The 5-fold surface of the monocrystalline *i*-Al-Pd-Mn was polished using a 0.25  $\mu$ m diamond paste before inserting it into the ultra-high vacuum chamber. The polished *i*-Al-Pd-Mn surface was treated *in-situ* by repeated cycles of Ar<sup>+</sup> ion sputtering at 1-2 keV for 30-60 min and annealing to 970 K for 2-2.5 hr to produce an atomically clean surface with a composition similar to the bulk [54, 55]. Gallium of 99.99% purity was evaporated using a water-cooled Knudsen cell [56] operating at 1050 K at a pressure better than  $2 \times 10^{-10}$  mbar. The substrate surface was freshly prepared for each deposition.

The DFT calculations to probe the interaction of Ga atoms with the *i*-Al-Pd-Mn surface were performed us-

ing the method of the Vienna Ab initio Simulation Package (VASP) [57–59]. The models of the surface have been derived from the Katz-Gratias-Boudard model [60] of bulk *i*-Al-Pd-Mn. The atomic structure of the 5-fold surface is derived from the icosahedral approximants by cleaving at a plane perpendicular to one of the 5-fold axes. Details of construction of the surface models can be found in our previous papers [40, 61–63]. The adsorption energy  $E_A[\text{Ga}]$  of Ga adatom is defined with respect to the energy in the crystalline structure as  $E_A[\text{Ga}] = E_{tot}[\text{Ga}] - E_{surf} + N_A \times \mu[\text{Ga}]$ , where  $E_{tot}$  is the energy of the *i*-Al-Pd-Mn surface model [40, 60] with the adsorbed adatoms.  $E_{surf}$  is the energy of the model *i*-Al-Pd-Mn surface representing the atomic structure of the clean quasicrystalline 5-fold surface.  $N_A$  is the number of adatoms in the cluster on the surface.  $\mu[\text{Ga}]$  is the chemical potential of Ga in the crystalline structure,  $\mu[\text{Ga}] = -E_{cryst}[\text{Ga.oP8}] = 2.934$  eV. The adsorption energy per atom  $E_a$  is  $E_a[\text{Ga}] = E_A[\text{Ga}]/N_A$ .

### III. RESULTS AND DISCUSSION

#### A. Nucleation of Ga on *i*-Al-Pd-Mn

A STM topography image for a deposition time ( $t_d$ ) of 2 min results in a coverage of 0.1 ML Ga on *i*-Al-Pd-Mn. The coverage is determined by the fraction of the total area covered by the Ga clusters that are identified by the bright regions in Fig. 1(a). The clusters have pentagonal symmetry that resembles flowers with five petals and are highlighted by white circles and ovals. We refer to these as Ga white flowers (GaWFs). The height of the GaWFs is determined by subtracting the average  $z$  corrugation of the substrate from that of the GaWF, as illustrated in Fig. 1(b). In Fig. S2(a) of the SM [51], a distribution of the heights obtained from several height profiles is fitted with a Gaussian function. The position of its maximum gives the average height of the GaWF to be  $0.18 \pm 0.03$  nm. A zoomed view of a GaWF motif is shown in Fig. 1(c). The length of the sides of the pentagon (white dashed lines) joining its petals has been determined for several motifs. Its average length turns out to be  $0.79 \pm 0.1$  nm, and the corresponding distribution is shown in Fig. S2(b) of SM [51].

To understand the origin of the GaWF, we have performed DFT calculation for the adsorption of Ga atoms on the 5-fold *i*-Al-Pd-Mn surface that was modeled as the 2/1 approximant [Fig. 1(d)]. The 5-fold *i*-Al-Pd-Mn surface is superposed with the Penrose P1 tiling (black lines) [61]. The P1 tiling has an edge length ( $a_0$ ) of 0.776 nm. The Mn atoms (red circles) appear at the centers of the pseudo-Mackay clusters (pMC). The vertices of the P1 pentagon are occupied by 5 Pd atoms (magenta circles). This figure shows that the surface Mn atoms are in the center of the P1 tiling, around which the well known white flower motifs of the substrate form [64, 65].

Quasicrystalline surfaces offer a greater number of inequivalent adsorption sites compared to ordinary crystals, allowing for the formation of various adatom configurations. On the 5-fold *i*-Al-Pd-Mn surface, there are two kinds of regular sites that preferably adsorb Ga atoms. The first site is the center of the surface 5-Al cluster that has a Pd atom. These Pd atoms can be 0.048 nm or 0.126 nm below the surface plane. Therefore, there are 2 kinds of the Pd sites and only one can adsorb the adatoms. The Ga atoms are adsorbed preferably only at the centers of the 5-Al cluster with the deeper Pd atom. These deeper Pd atoms are the centers of the Bergman clusters [60]. In Fig. 1(d), these sites are at the vertices of the P1 tiles and are also marked by white dots in Fig. 4(f) and Fig. S3(b) of SM. The binding energy of a single Ga atom in such sites is  $-1.357$  eV (see Table I). The second preferable adsorption site for a Ga adatom is the central Mn atom at the surface. The main reason for the higher reactivity of these Mn atoms is their low coordination: In the bulk pMC cluster, in the first shell around the Mn atom, there are only 7 nearest neighbors [60, 66]. The binding energy of Ga atoms at the surface Mn atoms is between  $-1.2$  eV and  $-1.4$  eV.

In previous studies [16, 37, 40, 55, 63, 66], it was observed that the adatoms (Bi, Pb, and Sn) form WF clusters around the surface Mn atoms. Our DFT calculations show that Ga atoms adsorbed on the 5-fold *i*-Al-Pd-Mn surface also form clusters similar to the previously observed WFs, but the internal structure is distinct because of the notably different electronic structure of Ga [41, 42]. In the previous studies [16, 37, 40, 55, 63, 66], the adatoms form the WF cluster, in which the outer and inner rings are oriented in the same direction and are therefore interconnected to form a starfish-like configuration. The GaWF cluster also consists of the outer ring of five Ga atoms, each adsorbed at the vertices of the P1 pentagon that are the centers of the reactive 5-Al clusters [Fig. 1(e)] that is the same as in the previous WFs. However, in contrast, the central pentagon of Ga adatoms has an opposite orientation compared to the pentagon of the atoms in the outer ring. Moreover, to stabilize this central pentagon, there must be an additional Ga atom at the center, making it a 6 atom Ga cluster (6-Ga), while retaining the pentagonal symmetry. The energies calculated for different Ga clusters are discussed later and compared in Table I. The opposite orientation of the pentagonal rings reflects the lower attractive interaction of adatoms between the outer ring and central 6-Ga cluster. In the case of the Ga adatoms, the outer and inner rings can also exist independently. The formation of the central 6-Ga cluster is slightly ( $-0.16$  eV/Ga atom) preferred over the formation of both rings simultaneously. The central Ga atom in the 6-Ga cluster is elevated by 0.1 nm compared to the five Ga neighbors. Therefore, the center of the GaWF cluster may appear brighter in the STM images than the outer ring. Also, on the 6-Ga cluster at the center, additional Ga atoms can be adsorbed, which can lead to a brighter center and

an irregular shape. We also note that, due to stochastic reasons, some GaWF motifs have a dark center, which could be caused by the absence of the 6-Ga cluster at the center.

It should be noted that the edge length of the P1 tiling  $a_0$  ( $= 0.776$  nm) is in excellent agreement with the side length of the GaWF from STM ( $0.79 \pm 0.1$  nm). Additionally, the typical distance between two neighboring Mn atoms on which the 6-Ga clusters are centered is  $1.255$  nm ( $= \tau \times a_0$ , where  $\tau = 1.618$ ). This distance also agrees well with the distance between the nearest neighbor GaWFs, as shown by the white ovals in Fig. 1(a), where the distance between their centers is  $\sim 1.25$  nm. This confirms that the 6-Ga clusters nucleate on the Mn atoms i.e., on the white flower motifs of the substrate.

TABLE I. Adsorption energies per atom  $E_a$  [eV] of Ga clusters consisting from  $N_A$  adatoms on the 5-fold *i*-Al-Pd-Mn surface.

	Single Ga	Outer 5-Ga	WF cluster	Inner 6-Ga
$N_A$	1	5	11	6
$E_a$	-1.357	-0.451	-0.354	-0.515

A comparison of the adsorption energies of Ga adatoms on the 5-fold *i*-Al-Pd-Mn surface are presented in Table I. As mentioned above, the adsorption energy of  $-1.357$  eV corresponds to a single Ga adatom adsorbing at the reactive center of the 5-Al surface cluster above the Pd atom. The adsorption energy per atom ( $E_a$ ) of the pentagonal 5-Ga outer ring of adatoms adsorbed in the five reactive 5-Al surface sites is  $-0.451$  eV. The GaWF cluster with an  $E_a$  of  $-0.354$  eV consists of the outer 5-Ga ring and the inner 6-Ga cluster. The  $E_a$  of the central 6-Ga cluster formed alone around the surface Mn atom is the strongest ( $-0.515$  eV). The adsorption of adatoms in the clusters is weaker compared to the adsorption of a single adatom because, in the cluster, in addition to bonding of adatoms to the surface, there are also interactions between the adatoms.

For comparison, in Discussion I of the SM, we also present the adsorption energies of the previously studied Sn white flower (SnWF) cluster [16] on the same 5-fold *i*-Al-Pd-Mn surface.  $E_a$  of the complete SnWF cluster is  $-0.795$  eV (see Table S1 of the SM), which is significantly larger than  $E_a = -0.354$  eV of the GaWF cluster. This could be a possible reason for the somewhat worse quality of the GaWF motifs [Fig. 1(a)] compared to the SnWF motifs on *i*-Al-Pd-Mn [see Fig. 10(a) and Fig. S8 of Ref. 16]. Another possible reason is that the STM in the present work has been performed at room temperature, which is close to the melting point of Ga, resulting in enhanced thermal effects.

The 5-fold surface of *i*-Al-Pd-Mn is primarily composed of Al atoms, with the top two atomic planes of the 5/3-approximant consisting of 75.9% Al, 19.6% Pd, and 4.5% Mn [66]. So, it can be interesting to compare the adsorption of Ga adatoms on the crystalline Al(111) sur-

face with the results in Table I for the quasicrystalline surface. Discussion II of SM [51] shows that the reactivity of the adsorption sites on *i*-Al-Pd-Mn is significantly higher compared to Al(111).

## B. Submonolayer Ga on *i*-Al-Pd-Mn

In Fig. 2(a), the deposition of Ga for  $t_d = 4$  minutes results in the formation of condensed islands with a lateral size of  $\sim 20$  nm. The coverage turns out to be 0.4 ML. The height profiles show that their height is similar to the GaWFs, indicating that islands constitute monolayer Ga (the distribution is shown in Fig. S2(c) [51]). The formation of such islands – in contrast to a dispersed phase reported for alkali metals on *i*-Al-Pd-Mn [36] – shows that the interaction between the adatoms is considerable.

It is interesting to note here that besides the GaWF motifs (white circles), larger sized white flower motifs [yellow circles in Fig. 2(a)] are observed. We refer to these as  $\tau$ -inflated GaWF or  $\tau$ -GaWF as their size scales with  $\tau$  compared to the GaWF motif. In addition, red circles highlight a larger, more complicated motif with a bright center and an outer ring of pentagons. We refer to it as the “ring” motif. In subsection III D, we elaborate on the origin of these motifs based on our DFT calculation.

To establish the quasiperiodic nature of the Ga adlayer at 0.4 ML coverage, in Fig. 2(b) we show the FFT of the Ga island regions of the STM image by masking the substrate using the height threshold procedure. The quasiperiodic nature of the islands is confirmed by the 10-fold FFT spots, with the angle subtended by two adjacent spots at the center being  $36^\circ \pm 2^\circ$ . In Fig. S4(a) of SM [51], the presence of all the spots is confirmed by the intensity profiles that show a peak that represents each spot.

The STM topography image in Fig. 2(c) shows that for 0.7 ML Ga coverage ( $t_d = 8$  min), the condensed islands grow larger in size and merge together. The  $\tau$ -inflated GaWF motifs (yellow circles) are more prevalent at this coverage. Additionally, their orientation is found to vary, as indicated by the yellow dashed pentagons that are rotated by  $36^\circ$ .

The FFT in Fig. 2(d) [see also Fig. S4(b) of SM [51]] for the Ga adlayer region displays 10-fold spots with the angle subtended at the center by the adjacent spots being  $36^\circ \pm 2^\circ$ . Thus, the FFT shows that the quasiperiodicity is retained up to this coverage. The height profiles taken along the red and orange dashed lines shown in Fig. 2(c) are plotted in Fig. 2(e). Considering several such height profiles, the average height turns out to be  $0.18 \pm 0.03$  nm, in agreement with that determined for 0.1-0.4 ML. Note that the thickness of the Ga monolayer is somewhat smaller compared to other quasiperiodic layers of elemental metals on *i*-Al-Pd-Mn, such as Sn (0.2 nm) [16] and Pb (0.23 nm) [38, 40]. A possible reason is the smaller

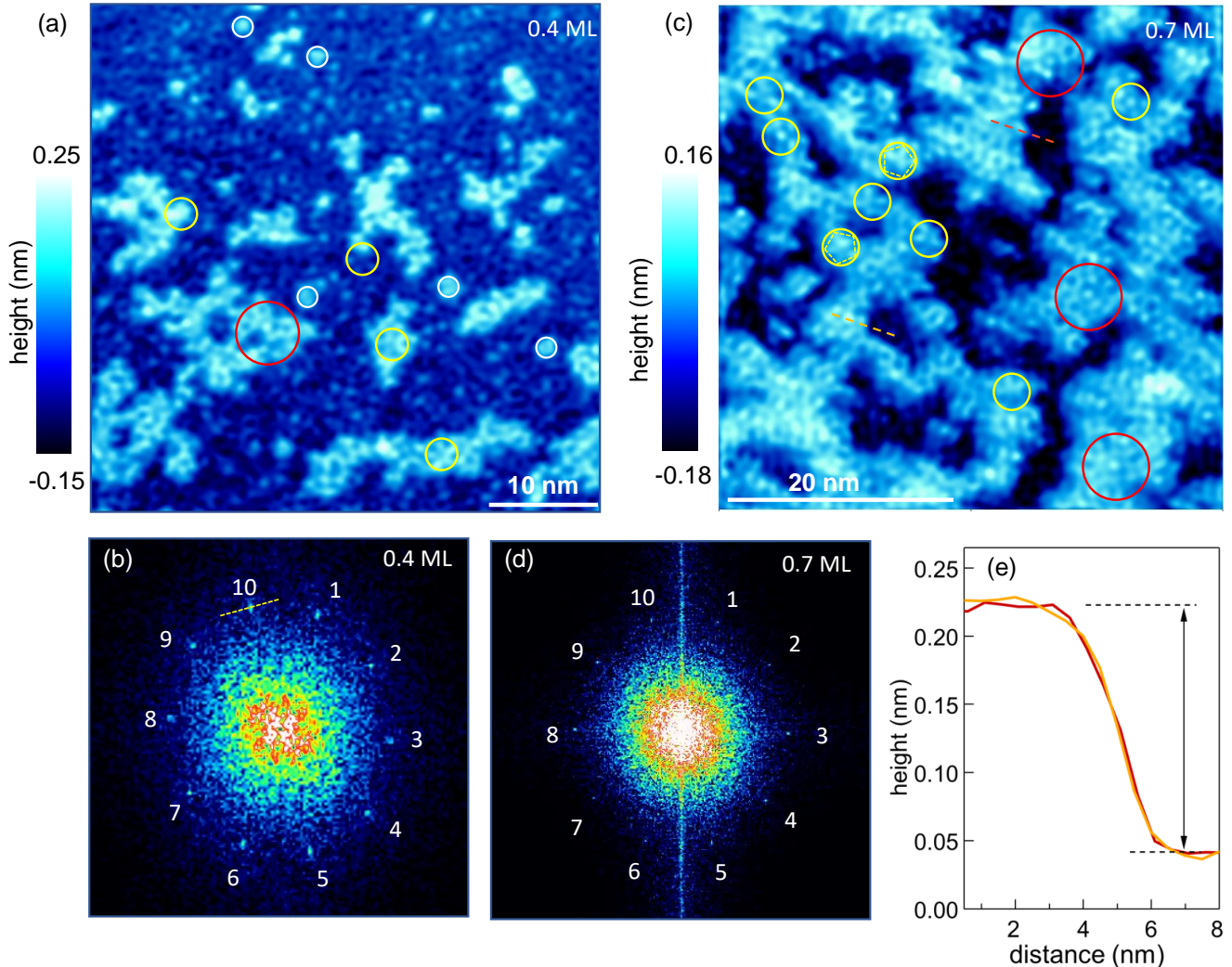


FIG. 2. (a) STM topography image of 0.4 ML Ga/*i*-Al-Pd-Mn ( $I_T = 0.5$  nA,  $U_T = 1.0$  V), where white, yellow, and red circles highlight the Ga white flower (GaWF),  $\tau$ -GaWF, and ring motifs, respectively. (b) Fast Fourier transform (FFT) calculated for panel a by selecting only the Ga islands and masking the substrate using the height threshold procedure, the spots are numbered as 1-10. (c) STM topography image of 0.7 ML Ga ( $I_T = 0.7$  nA,  $U_T = 0.9$  V), the motifs are highlighted as in panel a. (d) FFT of the Ga islands in panel c after masking the substrate with the spots numbered. (e) The height profile along the red and orange dashed lines in panel c.

size of the Ga atom (empirical atomic diameter being 0.26 nm [67]) compared to Sn (0.29 nm) and Pb (0.36 nm).

### C. Quasiperiodicity of monolayer gallium

Figure 3(a) illustrates the STM topography image for  $t_d = 16$  minutes, in which the substrate is uniformly covered by the Ga monolayer. Note that the characteristic quasiperiodic motifs such as  $\tau$ -GaWF and ring – similar to those observed in Fig. 2 – are also observed on the

Ga monolayer, these are highlighted by similar colored circles in Fig. 3(a).

Curiously, in this figure, isolated bright condensed islands are observed. In Fig. 3(d), the height profiles along the red and yellow dashed lines in Fig. 3(a) show that the average height of these islands relative to the monolayer is  $0.19 \pm 0.02$  nm. This is nearly similar to the monolayer's height discussed in the previous section, and thus the bright islands can be related to Ga bilayer regions. This is further supported by the height histogram in Fig. 3(e), which displays two peaks corresponding to the mono- and bilayer, the separation between which yields a sim-

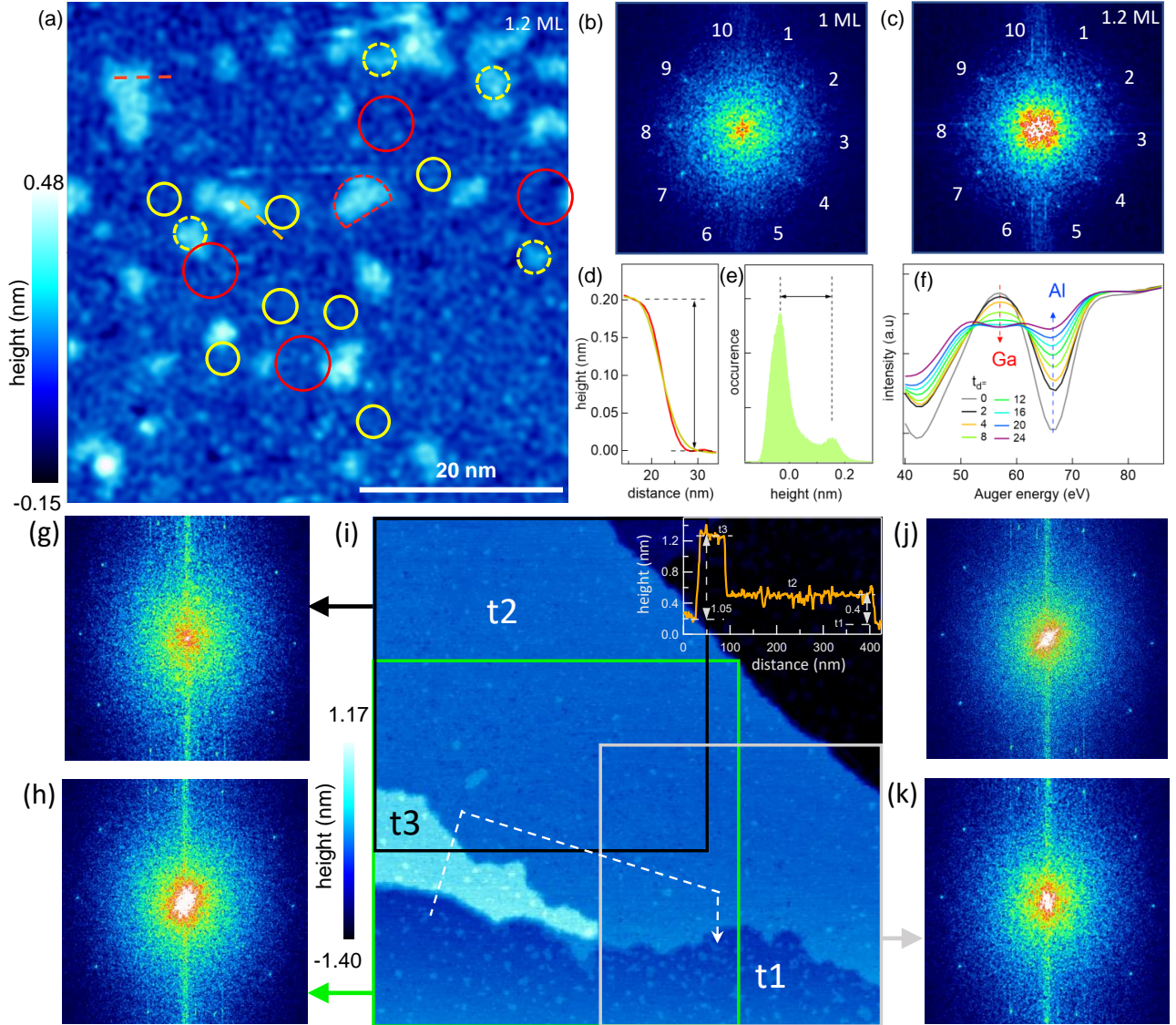


FIG. 3. (a) STM topography image of 1.2 ML Ga/*i*-Al-Pd-Mn ( $I_T = 0.8$  nA,  $U_T = 0.5$  V) showing formation of a uniform Ga monolayer. The motifs of the monolayer are highlighted by circles of similar color, as shown in Fig. 2. The motifs in the bright condensed islands that represent Ga bilayer regions are shown by dashed circles. FFT of (b) the monolayer region by masking the bilayer regions and (c) the whole image in panel a. (d) The height profile along the red and yellow dashed lines in panel a. (e) Height histogram of panel a. The double-sided black arrows in panels d and e indicate the thickness of the second Ga layer. (f) Auger electron spectra as a function of deposition time ( $t_d$ ) show an increase in the Ga *MNN* signal (red arrow) and a decrease in the Al *LMM* (blue arrow) signal. (i) A large area (250 nm $\times$ 250 nm) STM topography image of 1.2 ML Ga/*i*-Al-Pd-Mn ( $I_T = 0.6$  nA,  $U_T = -1.9$  V) and its (j) FFT. The inset of panel i shows the height profile along the white dashed line. FFT of the different regions of panel i, as indicated by the (g) black, (h) green, and (k) gray squares.

ilar height of the latter (horizontal double-sided arrow). From the area under the two peaks of the height histogram, we find that the bilayer forms over an area that is  $\approx 20\%$  of the total area. Thus, the coverage for this deposition turns out to be 1.2 ML.

Fig. 3(b) displays the FFT of only the monolayer (i.e.,

excluding the bilayer regions), while Fig. 3(c) displays the FFT of the entire image. 10-fold spots are observed in both. Notably, from a comparison of their intensity profiles in Fig. S5 of SM [51], it is apparent that the intensity of the spots is larger with the inclusion of the bilayer regions, indicating an improvement in the quality of the FFT. In addition, close scrutiny reveals the char-

acteristic quasiperiodic motifs such as  $\tau$ -GaWF and an incomplete ring on the bilayer islands [dashed circles in Fig. 3(a)], indicating the possible existence of quasiperiodic structural correlations in some regions of the bilayer.

In Fig. 3(f), the Ga MNN Auger electron spectroscopy signal at 55 eV increases with a concomitant decrease of the substrate Al LMM signal at 68 eV as a function of  $t_d$ . This shows that the Ga atoms are deposited incrementally on the *i*-Al-Pd-Mn surface. No change in the position of either of the peaks is observed over the whole  $t_d$  range (see the vertical dashed arrows), indicating the absence of any surface alloying or chemical bonding with the substrate.

A STM topography image in Fig. 3(i) for 1.2 monolayer coverage ( $t_d=16$  min) that spans a larger length scale (250nm $\times$ 250 nm) shows three adjacent terraces of the substrate. The bottom terrace is marked as t1 (blue), while the other terraces that exhibit step heights of  $0.4\pm 0.02$  nm ( $=L$ ) and  $1.05\pm 0.02$  nm ( $=2L+S$ ,  $L$  and  $S$  are the basic heights related by  $L=\tau\times S$ ) are referred to as t2 (light blue) and t3 (whitish blue), respectively; see the inset for the height profile along the white dashed line.  $L$  and  $(2L+S)$  are the characteristic step heights of the substrate [68–70]; their presence indicates that these terraces are uniformly covered by the Ga monolayer (the small bright isolated islands are the bilayer regions). The quasiperiodicity of Ga on these terraces is established by the presence of sharp 10-fold spots in the FFT, as shown in Fig. 3(g) for an overlapping area of t2 and t3 terraces (black square). In Fig. 3(h), FFT is shown for an overlapping area of all the three terraces (green square), while Fig. 3(k) shows it for t1 and t2 (gray square). The whole image also shows FFT spots [Fig. 3(j)]. Thus, the Ga monolayer is quasiperiodic over t1, t2, and t3 terraces, whose combined area is  $0.0525\ \mu\text{m}^2$ . The largest length scale over which quasiperiodicity is observed here is  $\sim 350$  nm, which is the diagonal of the image in Fig. 3(i). The signature of long range quasiperiodicity of the Ga monolayer is thus obtained over a range larger than the previous reports in the literature for other elements [15–17, 34, 37, 38].

#### D. DFT based models for the $\tau$ -GaWF and ring motifs

The STM images in Figs. 2-3 show that the  $\tau$ -GaWF motif with a dark center is most frequently observed, whose zoomed views are shown in Figs. 4(a,b). Some of these motifs are also observed with a bright center [Figs. 4(c)]. To show that these motifs are  $\tau$  inflated compared to the GaWF motifs, we determine the edge length of the pentagon shown by yellow dashed lines in Figs. 4(a-c). Its average value is  $1.26\pm 0.1$  nm, the corresponding distribution is shown in Fig. S6 of SM [51]. The experimental ratio of the side length of  $\tau$ -GaWF and the GaWF motifs

is  $\frac{1.26}{0.79}=1.59$ , which is close to  $\tau$  ( $=1.618$ ). Thus, STM shows that the  $\tau$ -GaWF motif is indeed  $\tau$  inflated with respect to the GaWF motif.

The size of this motif can be approximately estimated by the diameter of a circle circumscribing it drawn such that the  $\tau$ -GaWF motif is contained in it. The distribution of the diameter, considering several such motifs, is plotted as a histogram in Fig. S7(a) [51]. The average diameter of the  $\tau$ -GaWF motif turns out to be  $3.2\pm 0.2$  nm. This is approximately  $\tau$  scaled with respect to the diameter of the GaWF ( $2\pm 0.1$  nm), thus justifying the name “ $\tau$ -GaWF”.

Fig. 4(d) shows the atomic structure of the surface plane of the 5-fold *i*-Al-Pd-Mn derived from the 5/3 approximant. To model larger sized motifs by DFT, the  $\tau$ -P1 tiling is more appropriate (blue lines), where the size of the tiles is  $\tau$  times larger with the edge length  $a_1=1.255$  nm ( $=\tau\times a_0$ ,  $a_0=0.776$  nm) compared to the P1 tiling (black lines). Here, all the surface Mn atoms are at the vertices of the  $\tau$ -P1 tiling, but not all vertices of the  $\tau$ -P1 tiling are occupied by Mn atoms. In the central P1 pentagon, all 5 vertices are occupied by Mn atoms. At the center of this  $\tau$ -P1 pentagon, a dip can be observed. In previous studies, such a surface dip was also characterized also by a charge density minimum (see e.g., Fig. 3 in Ref. 63).

If around the Mn atoms of the  $\tau$ -P1 pentagon the 6-Ga clusters grow, a new Ga superstructure can be observed that would represent  $\tau$ -GaWF, as shown in Fig. 4(e). This model is supported by the excellent agreement of  $a_1$  estimated from the side length of the  $\tau$ -GaWF motifs from STM ( $1.26\pm 0.1$  nm) with the theoretical value (1.255 nm). Also, this model accurately reflects the distinct petals in the  $\tau$ -GaWF motif observed from STM. On *i*-Al-Pd-Mn surfaces, the dips could be filled by Ga adatoms, and the dark center of the  $\tau$ -GaWF could disappear. This could explain the bright centered  $\tau$ -GaWF motif in Figs. 2(c). On the *i*-Al-Pd-Mn surface,  $\tau$ -P1 pentagons with Mn atoms at all 5 vertices exist in varying orientations. This explains why  $\tau$ -GaWF clusters could be rotated relative to one another, as seen in Figs. 4(a,b) and Fig. 2(c).

A zoomed view of the ring motif (red circles in Figs. 2-3), which comprises of a nearly circular arrangement of outer pentagons, is shown in Fig. 4(g). The center of the ring motif is bright and is surrounded by a relatively darker region. An estimate of the average diameter of this motif is  $5.2\pm 0.4$  nm, indicating that it is approximately  $\tau$  inflated with respect to the  $\tau$ -GaWF motif (3.2 nm). The distribution of the diameters is shown in Fig. S7 [51].

In Fig. 4(f), we present a DFT based model of the ring motif that consists of an outer ring of pentagons formed by Ga atoms that occupy the favorable Pd sites at the middle of the 5-Al cluster that occur at the vertices of the pentagons of the P1 tiling shown by black lines. All possible favorable sites for Ga adsorption are shown by white

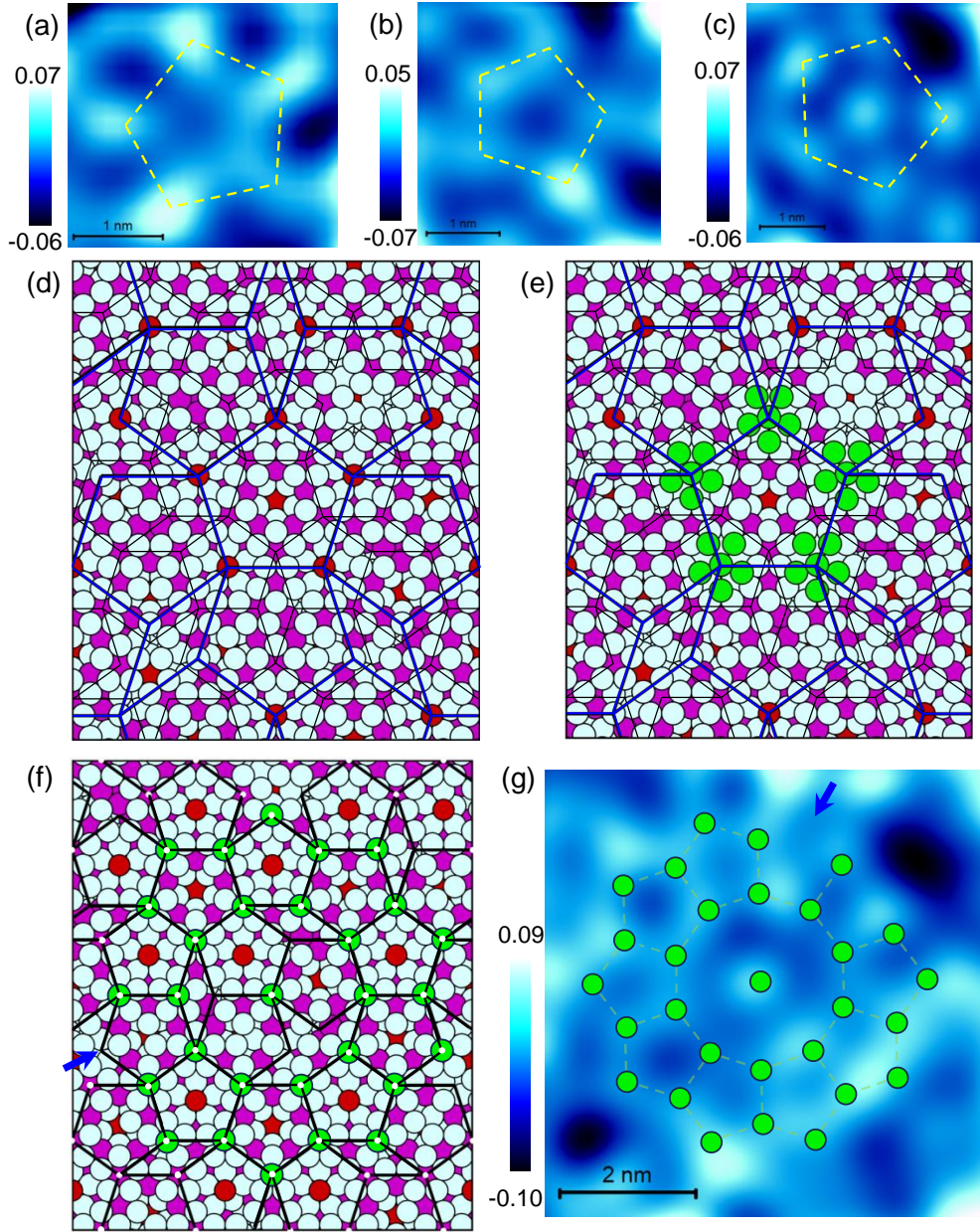


FIG. 4. Zoomed STM images of the  $\tau$ -GaWF motif with a dark center observed for the Ga (a) monolayer and (b) bilayer. (c) A  $\tau$ -GaWF motif with a bright center. The color scale representing the height in nm is shown on the left side of panels **a-c** and **f**, zero corresponds to the bearing height. (d) The atomic structure of the surface plane of 5-fold  $i$ -Al-Pd-Mn derived from the  $5/3$  approximant ( $5.32 \text{ nm} \times 6.25 \text{ nm}$ ), the thick blue (black) lines show the  $\tau$ -P1 (P1) tiling. The white, magenta, and red colored circles represent the Al, Pd, and Mn atoms, respectively. (e) Same as panel **d** with DFT based 30-Ga atom (green circles) model representing the  $\tau$ -GaWF motif on the  $i$ -Al-Pd-Mn surface. (f) A model for the ring motif, the white dots show all possible adsorption sites on the Pd atoms at the center of the 5-Al cluster. The blue arrow shows a vertex of the outer pentagon that is not a favorable site. The black lines show the P1 tiling that is shifted compared to panel **d**. (g) The green circles show the adsorbed Ga atoms of the model connected by green dashed lines overlaid on the zoomed ring motif from STM. Both panels **f** and **g** have same length scale.

dots in Fig. 4(f), while the green circles in Fig. S3(c) of SM represent a complete ring motif. The bright center of the ring motif also arises from a Ga adatom adsorbed at the center Pd atom surrounded by the 5-Al cluster.

This is the common vertex of three inner P1 pentagons, however two vertices of each of these pentagons are not energetically favorable. To be noted is that 6-Ga clusters on the Mn atoms at the center of the alternate pentagons



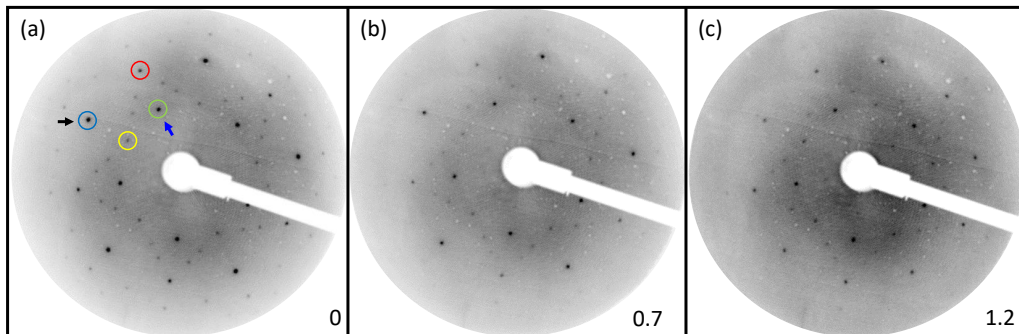


FIG. 5. LEED patterns at a beam energy ( $E_p$ ) of 81 eV for (a) 0, (b) 0.7, and (c) 1.2 ML Ga/*i*-Al-Pd-Mn in an inverted gray scale, the coverage is indicated at the bottom right corner of each panel.

could form a GaWF, but it is somewhat energetically less favored compared to only the outer 5-Ga considered in the model (Table I). A satisfactory agreement can be noticed in both the atomic positions and motif size when this model is superimposed on the ring motif depicted in Fig. 4(g) subsequent to a  $120^\circ$  rotation. It is worth noting that the majority of the vertices comprising the outer ring of 10 pentagons are energetically favorable (as indicated by white dots). However, there is one unfavorable vertex, denoted by a blue arrow in Figs. 4(f,g), which lacks both the Pd atom and the 5-Al cluster. Additionally, a neighboring vertex of the ring motif in Fig. 4(g) is unoccupied for stochastic reasons.

### E. Low energy electron diffraction study of Ga/*i*-Al-Pd-Mn

Figure 5(a) displays the LEED pattern of *i*-Al-Pd-Mn that has different sets of sharp 5-fold spots in agreement with the literature [16, 39, 71]. The most intense inner and outer sets of spots are indicated by blue and black arrows, respectively. These spots with similar relative intensities between the 5-fold sets are clearly visible for 1.2 ML coverage in Fig. 5(c)], where the surface is uniformly covered by Ga, as shown by STM in Fig. 3, also see Fig. S8 for other  $E_p$  values. The spots are also visible for the submonolayer coverage of 0.7 ML [Figs. 5(b)]. The intensity profiles of the inner and outer sets of spots for 1.2 ML LEED pattern in Fig. S9(a) of SM [51] show that the angular position (separation between spots being  $36^\circ \pm 1^\circ$ ) and the width of the spots remain nearly unchanged with respect to the substrate. The profiles along three radial directions in Figs. S9(b-d) show similar  $k_{||}$  for both sets of spots, indicating an unchanged quasi-lattice parameter of the Ga adlayer compared to the substrate. There is no evidence of splitting or broadening of the spots indicating the absence of surface defects or steps of multiple heights [72]. It may be noted that rotational epitaxy instead of quasiperiodicity has been reported for several metals deposited on *i*-Al-Pd-Mn such as Al [73],

Ag [74], Fe [75], and Ni [76]. In these cases, the adlayer manifests as five crystalline domains that mirror the symmetry of the substrate, and these domains add extra spots to the LEED pattern. Such extra spots are absent for the Ga monolayer for the whole  $E_p$  range, as shown by a series of patterns from  $30 \text{ eV} < E_p < 180 \text{ eV}$  at a step of 2 eV in video files named “Ga0.7ML” and “Ga1.2ML” for 0.7 and 1.2 ML, respectively of the SM [51]. This rules out the possibility of the formation of Ga domains with a particular orientational relationship with the substrate. Thus, our electron diffraction study shows that the Ga monolayer exhibits quasiperiodic order within the coherence length scale of the LEED optics, which is 10-20 nm [77]. There is however a decrease in the intensity of the Ga adlayer spots, indicating an increase in disorder and roughness. This statement is supported by the fact that the roughness of the monolayer (0.05 nm), as measured by STM, is larger compared to the substrate (0.02 nm).

Although the LEED patterns of the Ga adlayer resemble the substrate in Fig. 5, for some  $E_p$ , the relative intensities of the two sets of 5 fold spots are different [Figs. 6(a-f)]. For example, at  $E_p = 55 \text{ eV}$  in Fig. 6(d), the outer ring has nearly equal intensities of the two sets (thus appearing like a decagon, red lines), while for the substrate in Fig. 6(a) one set is more intense compared to the other (thus appearing as two  $36^\circ$  rotated pentagons, shown by solid and dashed red lines). This is also observed at 86 eV. Moreover, at 55 eV, the inner pentagon highlighted by blue lines is  $36^\circ$  rotated between the two. At 63 eV, the inner (outer) set of spots of the Ga layer portrays a blue (solid and dashed red) pentagon, while for the substrate, the spots are of equal intensity.

To understand these differences, the intensity ( $I$ ) of a LEED spot as a function of  $E_p$  – called  $I$ - $V$  curve [72, 78] – has been shown in Figs. 6(g-j). The  $I$ - $V$  curves of the substrate for different spots, such as (10000), (11000), (00010), and (00110) are in agreement with the earlier reports [16, 79]. Although a comparison with the substrate shows a fair qualitative closeness in the positions

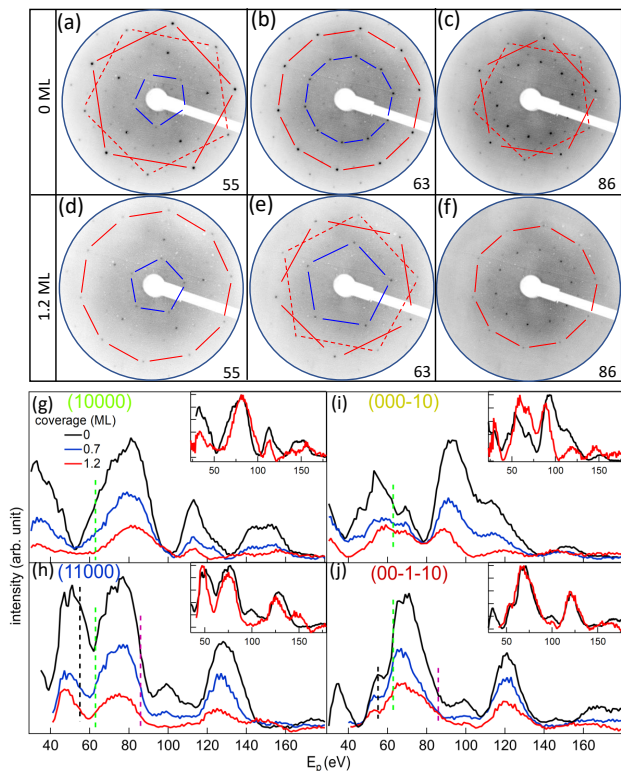


FIG. 6. LEED patterns of (a-c) *i*-Al-Pd-Mn, and (d-f) 1.2 ML Ga/*i*-Al-Pd-Mn for three different  $E_p$  values are shown at the bottom right corner in eV. The differences are highlighted by blue and red lines. Experimental  $I$ - $V$  curves for 0.7 and 1.2 ML Ga/*i*-Al-Pd-Mn compared with *i*-Al-Pd-Mn (0 ML) for different spots (g) (10000), (h) (11000), (i) (000 $\bar{1}$ 0), and (j) (00 $\bar{1}$  $\bar{1}$ 0). These spots are marked in Fig. 5(a) by green, blue, yellow, and red circles, respectively. The insets compare the 1.2 ML  $I$ - $V$  with the substrate after normalizing the most intense peak to the same height.

of the main peaks, there are perceptible differences in particular for (000 $\bar{1}$ 0) and (11000) spots, which are apparent in the insets where their most intense peak has been normalized to the same height. The difference in the shapes of the  $I$ - $V$  curves could arise from the structural difference caused by preferred adsorption positions of Ga on *i*-Al-Pd-Mn as shown by DFT as well as non-structural parameters such as change in the surface potential [72]. The differences in the LEED patterns between the Ga adlayer and the substrate in Figs. 6(a-f) can be explained by the difference in the shapes of the  $I$ - $V$  curves [dashed lines in Figs. 6(g-j)].

#### IV. CONCLUSIONS

In conclusion, our present study utilizing scanning tunneling microscopy (STM), low energy electron diffrac-

tion (LEED), and density functional theory (DFT) demonstrates that Ga monolayer on *i*-Al-Pd-Mn exhibits quasiperiodic order at room temperature. The FFTs of the STM images exhibit the characteristic quasiperiodic spots, while the real space images reveal motifs such as Ga white flower (GaWF) and  $\tau$ -inflated GaWF ( $\tau$ -GaWF), where  $\tau$  is the golden mean. A larger sized ring motif made up of pentagons in a circular congregation with a bright center is also observed. STM shows that the quasiperiodic order persists over a length scale of  $\sim 350$  nm. The quasiperiodic nature of the Ga monolayer is further supported by the 5-fold LEED patterns observed across the entire range of the beam energy. Auger electron spectroscopy provides additional evidence that the Ga adlayer does not exhibit any surface alloying or chemical reactions with the substrate.

Our DFT calculations indicate that Ga prefers to adsorb on *i*-Al-Pd-Mn at two specific sites: (i) the vertices of the Penrose P1 tile located at the center of a cluster consisting of 5 Al atoms that has a Pd atom at the center but positioned below the surface plane, and (ii) the Mn atom positioned at the center of the P1 tile. The GaWF motif is represented by a pentagonal outer ring comprising 5 Ga atoms adsorbed at the center of 5-Al clusters and a pentagonal inner cluster consisting of 6 Ga atoms (6-Ga) surrounding the central Mn atom. The 6-Ga clusters arranged on the  $\tau$ -P1 tiling serve as a model for the  $\tau$ -GaWF motif, while the ring motif is represented by Ga atoms that adsorb at the reactive centers of 5-Al clusters above the marked Pd sites. Excellent agreement is observed between the side length and the diameter of the motifs between the experiment and the DFT-based models. Our research reveals a previously unknown characteristic of gallium, i.e., its quasicrystallinity. It is intriguing that Ga exhibits quasiperiodic order despite the substrate temperature being near its melting point; this characteristic sets it apart from other systems.

#### V. ACKNOWLEDGMENTS

M.K. is thankful for the support from the Slovak Grant Agency VEGA (No. 2/0144/21) and APVV (No. 19-0369). We are grateful to M. Mihalkovič and K. Pussi for insightful discussions. We thank D. L. Schlager and T. A. Lograsso for providing us with the *i*-Al-Pd-Mn substrate. Special appreciation is extended to V. K. Singh for his suggestions regarding the STM measurement.

e-mail addresses:

\*marian.krajci@savba.sk,

†barmansr@gmail.com

- [1] R. Penrose, *Bull. Inst. Math. Appl.* **10**, 266 (1974).
- [2] D. Levine and P. J. Steinhardt, *Physical Review Letters* **53**, 2477 (1984).
- [3] D. Shechtman, I. Blech, D. Gratias, and J. W. Cahn, *Physical Review Letters* **53**, 1951 (1984).
- [4] A. P. Tsai, J. Q. Guo, E. Abe, H. Takakura, and T. J. Sato, *Nature* **408**, 537 (2000).
- [5] D. V. Talapin, E. V. Shevchenko, M. I. Bodnarchuk, X. Ye, J. Chen, and C. B. Murray, *Nature* **461**, 964 (2009).
- [6] S. Fischer, A. Exner, K. Zielske, J. Perlich, S. Deloudi, W. Steurer, P. Lindner, and S. Förster, *Proceedings of the National Academy of Sciences* **108**, 1810 (2011).
- [7] S. Förster, K. Meinel, R. Hammer, M. Trautmann, and W. Widdra, *Nature* **502**, 215 (2013).
- [8] C. Xiao, N. Fujita, K. Miyasaka, Y. Sakamoto, and O. Terasaki, *Nature* **487**, 349 (2012).
- [9] X. Ye, J. Chen, M. E. Irrgang, M. Engel, A. Dong, S. C. Glotzer, and C. B. Murray, *Nature Materials* **16**, 214 (2016).
- [10] W. Yao, E. Wang, C. Bao, Y. Zhang, K. Zhang, K. Bao, C. K. Chan, C. Chen, J. Avila, M. C. Asensio, J. Zhu, and S. Zhou, *Proceedings of the National Academy of Sciences* **115**, 6928 (2018).
- [11] S. J. Ahn, P. Moon, T.-H. Kim, H.-W. Kim, H.-C. Shin, E. H. Kim, H. W. Cha, S.-J. Kahng, P. Kim, M. Koshino, Y.-W. Son, C.-W. Yang, and J. R. Ahn, *Science* **361**, 782 (2018).
- [12] M. Maniraj, L. Lyu, S. Mousavion, S. Becker, S. Emmerich, D. Jungkenn, D. L. Schlagel, T. A. Lograsso, S. R. Barman, S. Mathias, B. Stadtmüller, and M. Aeschlimann, *New Journal of Physics* **22**, 093056 (2020).
- [13] J. D. Cain, A. Azizi, M. Conrad, S. M. Griffin, and A. Zettl, *Proceedings of the National Academy of Sciences* **117**, 26135 (2020).
- [14] K. J. Franke, H. R. Sharma, W. Theis, P. Gille, P. Ebert, and K. H. Rieder, *Physical Review Letters* **89**, 10.1103/physrevlett.89.156104 (2002).
- [15] H. R. Sharma, K. Nozawa, J. A. Smerdon, P. J. Nugent, I. McLeod, V. R. Dhanak, M. Shimoda, Y. Ishii, A. P. Tsai, and R. McGrath, *Nature Communications* **4**, 10.1038/ncomms3715 (2013).
- [16] V. K. Singh, M. Mihalkovič, M. Krajčí, S. Sarkar, P. Sadhukhan, M. Maniraj, A. Rai, K. Pussi, D. L. Schlagel, T. A. Lograsso, A. K. Shukla, and S. R. Barman, *Physical Review Research* **2**, 10.1103/physrevresearch.2.013023 (2020).
- [17] V. K. Singh, E. Pospíšilová, M. Mihalkovič, M. Krajčí, P. Bhakuni, S. Sarkar, K. Pussi, D. L. Schlagel, T. A. Lograsso, P. C. Canfield, and S. R. Barman, *Physical Review B* **107**, 10.1103/physrevb.107.045410 (2023).
- [18] L. Bindi, J. M. Eiler, Y. Guan, L. S. Hollister, G. MacPherson, P. J. Steinhardt, and N. Yao, *Proceedings of the National Academy of Sciences* **109**, 1396 (2012).
- [19] L. Bindi, M. A. Pasek, C. Ma, J. Hu, G. Cheng, N. Yao, P. D. Asimow, and P. J. Steinhardt, *Proceedings of the National Academy of Sciences* **120**, 10.1073/pnas.2215484119 (2022).
- [20] S. Poon, *Advances in Physics* **41**, 303 (1992).
- [21] S. Kang, J. Dubois, and J. von Stebut, *Journal of Materials Research* **8**, 2471 (1993).
- [22] J.-M. Dubois, S. S. Kang, and A. Perrot, *Materials Science and Engineering: A* **179-180**, 122 (1994).
- [23] J. Y. Park, D. F. Ogletree, M. Salmeron, R. A. Ribeiro, P. C. Canfield, C. J. Jenks, and P. A. Thiel, *Science* **309**, 1354 (2005).
- [24] J.-M. Dubois, *Chemical Society Reviews* **41**, 6760 (2012).
- [25] J. Hafner and M. Krajčí, *Physical Review Letters* **68**, 2321 (1992).
- [26] J. Nayak, M. Maniraj, A. Rai, S. Singh, P. Rajput, A. Gloskovskii, J. Zegenhagen, D. L. Schlagel, T. A. Lograsso, K. Horn, and S. R. Barman, *Physical Review Letters* **109**, 10.1103/physrevlett.109.216403 (2012).
- [27] J. Nayak, M. Maniraj, A. Gloskovskii, M. Krajčí, S. Sebastian, I. R. Fisher, K. Horn, and S. R. Barman, *Physical Review B* **91**, 10.1103/physrevb.91.235116 (2015).
- [28] S. Sarkar, P. Sadhukhan, V. K. Singh, A. Gloskovskii, K. Deguchi, N. Fujita, and S. R. Barman, *Physical Review Research* **3**, 10.1103/physrevresearch.3.013151 (2021).
- [29] R. Chen, C.-Z. Chen, J.-H. Gao, B. Zhou, and D.-H. Xu, *Physical Review Letters* **124**, 10.1103/physrevlett.124.036803 (2020).
- [30] J. Fan and H. Huang, *Frontiers of Physics* **17**, 10.1007/s11467-021-1100-y (2021).
- [31] C. Wang, F. Liu, and H. Huang, *Physical Review Letters* **129**, 10.1103/physrevlett.129.056403 (2022).
- [32] S. Sarkar, M. Krajčí, P. Sadhukhan, V. K. Singh, A. Gloskovskii, P. Mandal, V. Fournée, M.-C. de Weerd, J. Ledieu, I. R. Fisher, and S. R. Barman, *Physical Review B* **103**, 10.1103/physrevb.103.1241106 (2021).
- [33] T. Cai, J. Ledieu, R. McGrath, V. Fournée, T. Lograsso, A. Ross, and P. Thiel, *Surface Science* **526**, 115 (2003).
- [34] M. Shimoda, J. Guo, T. Sato, and A.-P. Tsai, *Journal of Non-Crystalline Solids* **334-335**, 505 (2004).
- [35] J. Ledieu, J. T. Hoeft, D. E. Reid, J. A. Smerdon, R. D. Diehl, N. Ferralis, T. A. Lograsso, A. R. Ross, and R. McGrath, *Physical Review B* **72**, 10.1103/physrevb.72.035420 (2005).
- [36] A. K. Shukla, R. S. Dhaka, C. Biswas, S. Banik, S. R. Barman, K. Horn, P. Ebert, and K. Urban, *Physical Review B* **73**, 10.1103/physrevb.73.054432 (2006).
- [37] J. A. Smerdon, J. K. Parle, L. H. Wearing, T. A. Lograsso, A. R. Ross, and R. McGrath, *Physical Review B* **78**, 10.1103/physrevb.78.075407 (2008).
- [38] J. Ledieu, L. Leung, L. H. Wearing, R. McGrath, T. A. Lograsso, D. Wu, and V. Fournée, *Physical Review B* **77**, 10.1103/physrevb.77.073409 (2008).
- [39] A. K. Shukla, R. S. Dhaka, S. W. D'Souza, S. Singh, D. Wu, T. A. Lograsso, M. Krajčí, J. Hafner, K. Horn, and S. R. Barman, *Physical Review B* **79**, 10.1103/physrevb.79.134206 (2009).
- [40] J. Ledieu, M. Krajčí, J. Hafner, L. Leung, L. H. Wearing, R. McGrath, T. A. Lograsso, D. Wu, and V. Fournée, *Physical Review B* **79**, 10.1103/physrevb.79.165430 (2009).
- [41] J. Hafner and W. Jank, *Physical Review B* **42**, 11530 (1990).
- [42] S. R. Barman and D. D. Sarma, *Physical Review B* **51**, 4007 (1995).
- [43] V. Kochat, A. Samanta, Y. Zhang, S. Bhowmick, P. Man-

- imunda, S. A. S. Asif, A. S. Stender, R. Vajtai, A. K. Singh, C. S. Tiwary, and P. M. Ajayan, *Science Advances* **4**, [10.1126/sciadv.1701373](#) (2018).
- [44] M.-L. Tao, Y.-B. Tu, K. Sun, Y.-L. Wang, Z.-B. Xie, L. Liu, M.-X. Shi, and J.-Z. Wang, *2D Materials* **5**, [035009](#) (2018).
- [45] S. V. Badalov, M. Yagmurcukardes, F. M. Peeters, and H. Sahin, *The Journal of Physical Chemistry C* **122**, [28302](#) (2018).
- [46] S. Wundrack, D. Momeni, W. Dempwolf, N. Schmidt, K. Pierz, L. Michaliszyn, H. Spende, A. Schmidt, H. W. Schumacher, R. Stosch, and A. Bakin, *Physical Review Materials* **5**, [10.1103/physrevmaterials.5.024006](#) (2021).
- [47] A. Kutana, T. Altalhi, Q. Ruan, J.-J. Zhang, E. S. Penev, and B. I. Yakobson, *Nanoscale Advances* **4**, [1408](#) (2022).
- [48] Y. Jelialzova and R. Franchy, *Surface Science* **527**, [57](#) (2003).
- [49] R. Tran, Z. Xu, B. Radhakrishnan, D. Winston, W. Sun, K. A. Persson, and S. P. Ong, *Scientific Data* **3**, [10.1038/sdata.2016.80](#) (2016).
- [50] J.-M. Dubois, M.-C. de Weerd, J. Brenner, M. Sales, G. Mozdzen, A. Merstallinger, and E. Belin-Ferré, *Philosophical Magazine* **86**, [797](#) (2006).
- [51] See Supplemental Material for a Table S1, two Discussions I-II, Figs. S1 - S10, and two video files showing LEED as a function of electron energy.
- [52] P. Sadhukhan, S. Barman, T. Roy, V. K. Singh, S. Sarkar, A. Chakrabarti, and S. R. Barman, *Physical Review B* **100**, [10.1103/physrevb.100.235404](#) (2019).
- [53] A. Mayer, H. Salopaasi, K. Pussi, and R. D. Diehl, *Computer Physics Communications* **183**, [1443](#) (2012).
- [54] V. Fournée, P. J. Pinhero, J. W. Anderegg, T. A. Lograsso, A. R. Ross, P. C. Canfield, I. R. Fisher, and P. A. Thiel, *Physical Review B* **62**, [14049](#) (2000).
- [55] M. Maniraj, A. Rai, S. R. Barman, M. Krajčič, D. L. Schlagel, T. A. Lograsso, and K. Horn, *Physical Review B* **90**, [10.1103/physrevb.90.115407](#) (2014).
- [56] A. K. Shukla, S. Banik, R. S. Dhaka, C. Biswas, S. R. Barman, and H. Haak, *Review of Scientific Instruments* **75**, [4467](#) (2004).
- [57] G. Kresse and J. Furthmüller, *Computational Materials Science* **6**, [15](#) (1996).
- [58] G. Kresse and J. Furthmüller, *Physical Review B* **54**, [11169](#) (1996).
- [59] G. Kresse and D. Joubert, *Physical Review B* **59**, [1758](#) (1999).
- [60] M. Krajčič, M. Windisch, J. Hafner, G. Kresse, and M. Mi-halkovič, *Physical Review B* **51**, [17355](#) (1995).
- [61] M. Krajčič, J. Hafner, J. Ledieu, and R. McGrath, *Physical Review B* **73**, [10.1103/physrevb.73.024202](#) (2006).
- [62] M. Krajčič and J. Hafner, *Physical Review B* **77**, [10.1103/physrevb.77.134202](#) (2008).
- [63] M. Krajčič, J. Hafner, J. Ledieu, V. Fournée, and R. McGrath, *Physical Review B* **82**, [10.1103/physrevb.82.085417](#) (2010).
- [64] Z. Papadopoulos, G. Kasner, J. Ledieu, E. J. Cox, N. V. Richardson, Q. Chen, R. D. Diehl, T. A. Lograsso, A. R. Ross, and R. McGrath, *Physical Review B* **66**, [10.1103/physrevb.66.184207](#) (2002).
- [65] L. Barbier, D. L. Floc'h, Y. Calvayrac, and D. Gratias, *Physical Review Letters* **88**, [10.1103/physrevlett.88.085506](#) (2002).
- [66] M. Krajčič and J. Hafner, *Physical Review B* **71**, [10.1103/physrevb.71.184207](#) (2005).
- [67] J. C. Slater, *The Journal of Chemical Physics* **41**, [3199](#) (1964).
- [68] H. R. Sharma, M. Shimoda, and A. P. Tsai, *Advances in Physics* **56**, [403–464](#) (2007).
- [69] T. M. Schaub, D. E. Bürgler, H. J. Güntherodt, and J. B. Suck, *Physical Review Letters* **73**, [1255](#) (1994).
- [70] Z. Shen, C. R. Stoldt, C. J. Jenks, T. A. Lograsso, and P. A. Thiel, *Physical Review B* **60**, [14688–14694](#) (1999).
- [71] M. Gierer, M. A. V. Hove, A. I. Goldman, Z. Shen, S.-L. Chang, C. J. Jenks, C.-M. Zhang, and P. A. Thiel, *Physical Review Letters* **78**, [467](#) (1997).
- [72] M. A. V. Hove and S. Y. Tong, in *Springer Series in Chemical Physics* (Springer Berlin Heidelberg, 1979) pp. 251–266.
- [73] B. Bolliger, V. E. Dmitrienko, M. Erbudak, R. Lüscher, H.-U. Nissen, and A. R. Kortan, *Physical Review B* **63**, [10.1103/physrevb.63.052203](#) (2001).
- [74] V. Fournée, T. C. Cai, A. R. Ross, T. A. Lograsso, J. W. Evans, and P. A. Thiel, *Physical Review B* **67**, [10.1103/physrevb.67.033406](#) (2003).
- [75] Y. Weisskopf, R. Lüscher, and M. Erbudak, *Surface Science* **578**, [35](#) (2005).
- [76] Y. Weisskopf, M. Erbudak, J.-N. Longchamp, and T. Michlmayr, *Surface Science* **600**, [2594](#) (2006).
- [77] K. Hattori, K. Ishihara, Y. Miyatake, F. Matsui, S. Takeda, H. Daimon, and F. Komori, *Surface Science* **525**, [57](#) (2003).
- [78] K. Heinz, *Reports on Progress in Physics* **58**, [637](#) (1995).
- [79] M. Heinzig, C. J. Jenks, M. V. Hove, I. Fisher, P. Canfield, and P. A. Thiel, *Journal of Alloys and Compounds* **338**, [248](#) (2002).